

Electromagnetized gold nanoparticles mediate direct lineage reprogramming into induced dopamine neurons *in vivo* for Parkinson's disease therapy

Junsang Yoo¹, Euiyeon Lee², Hee Young Kim³, Dong-ho Youn⁴, Junghyun Jung⁵, Hongwon Kim¹, Yujung Chang¹, Wonwoong Lee⁶, Jaein Shin¹, Soonbong Baek¹, Wonhee Jang⁴, Won Jun⁴, Soochan Kim⁷, Jongki Hong⁶, Hi-Joon Park⁸, Christopher J. Lengner⁹, Sang Hyun Moh¹⁰, Youngeun Kwon² and Jongpil Kim^{1*}

Electromagnetic fields (EMF) are physical energy fields generated by electrically charged objects, and specific ranges of EMF can influence numerous biological processes, which include the control of cell fate and plasticity. In this study, we show that electromagnetized gold nanoparticles (AuNPs) in the presence of specific EMF conditions facilitate an efficient direct lineage reprogramming to induced dopamine neurons *in vitro* and *in vivo*. Remarkably, electromagnetic stimulation leads to a specific activation of the histone acetyltransferase Brd2, which results in histone H3K27 acetylation and a robust activation of neuron-specific genes. *In vivo* dopaminergic neuron reprogramming by EMF stimulation of AuNPs efficiently and non-invasively alleviated symptoms in mouse Parkinson's disease models. This study provides a proof of principle for EMF-based *in vivo* lineage conversion as a potentially viable and safe therapeutic strategy for the treatment of neurodegenerative disorders.

Electromagnetic force is a physical energy that occurs in the presence of an electromagnetic field (EMF) between electrically charged objects^{1,2}. Several lines of evidence show that an EMF has significant effects on various cellular processes, which include potentiating epigenetic reprogramming to pluripotency by the forced expression of transcription factors^{3–7}. The observation that EMF promotes epigenetic changes that influence the cell-fate conversion in a non-invasive, controllable manner raises the possibility of the therapeutic utilization of EMF in regenerative medicine.

Direct lineage reprogramming (conversion of one somatic cell type into another) is associated with major changes in gene-expression programmes mediated by extensive epigenetic alterations^{8–12}. Such reprogramming is traditionally driven by a forced expression of lineage-specific pioneer transcription factors and/or chromatin-modifying enzymes. Particularly, the direct *in vivo* reprogramming of abundant and readily accessible somatic cell types into induced dopaminergic (iDA) neurons represents a promising therapeutic strategy for Parkinson's disease (PD)^{12,13}. However, the development of safe and efficient lineage-conversion strategies remains a significant challenge as the genomic integration of reprogramming cassettes and low reprogramming efficiencies are major barriers to therapeutic applications^{12–14}.

Here we show that electromagnetic energy promotes the efficient conversion of somatic fibroblasts into iDA neurons both *in vitro* and

in vivo. Gold nanoparticles (AuNPs) exposed to specific EMF frequencies become transiently magnetized, which enables a more-direct transfer of EMF energy to the target cells. We demonstrate that AuNPs exposed to an EMF promote the induction of the histone acetyltransferase (HAT) Brd2, which acetylates histone H3K27 and leads to chromatin opening, the potentiation of neuronal gene expression and a dramatic improvement in neuronal reprogramming efficiency both *in vitro* and *in vivo*. As AuNPs are safe conductive biocompatible materials¹⁵, our findings may represent a viable therapeutic strategy for the restoration of the dopaminergic neuron function in PD.

Results

Preparation of electromagnetized AuNPs. We initially tested whether EMF exposure influences the generation of iDA neurons from mouse tail-tip fibroblasts (TTFs) that express ectopically the DA lineage transcription factors (and iDA reprogramming factors) Ascl1, Pitx3, Lmx1a and Nurr1 (APLN)¹². We prepared a culture substrate that contained thiol-capped AuNPs capable of magnetization on EMF exposure. We modified the AuNPs with two thiol-containing ligands, mercapto(methoxypolyethylene glycol) (mPEG₃₅₀-SH) and a heptapeptide, CYGRGDS. Thiol ligands were chosen as they form stable bonds with Au to induce magnetic polarization by the 'Fermi hole effect'. The PEG group

¹Laboratory of Stem Cells and Cell Reprogramming, Department of Biomedical Engineering (BK21 plus program), Dongguk University, Seoul 100-715, Republic of Korea. ²Laboratory of Protein Engineering, Department of Biomedical Engineering, Dongguk University, Seoul 100-715, Republic of Korea.

³Department of Physiology, College of Korean Medicine, Daegu Haany University, Daegu 45158, Republic of Korea. ⁴Department of Oral Physiology, School of Dentistry, Kyungpook National University, 2177, Dalgubeol Boulevard, Jung-gu, Daegu 41940, Republic of Korea. ⁵Department of Life Science, Dongguk University, Seoul 100-715, Republic of Korea. ⁶College of Pharmacy, Kyung Hee University, Seoul 02447, Korea. ⁷Department of Electrical and Electronic Engineering, Hankyong National University, Kyonggi-do 456-749, Republic of Korea. ⁸Studies of Translational Acupuncture Research (STAR), Acupuncture & Meridian Science Research Center (AMSRC), Kyung Hee University, 26 Kyungheedaero, Dongdaemoon-gu, Seoul 130-701, Republic of Korea.

⁹Department of Biomedical Sciences, School of Veterinary Medicine and Institute for Regenerative Medicine, University of Pennsylvania, Philadelphia, Pennsylvania 19104, USA. ¹⁰BIO-FD&C Co. 509-511, Smart Valley A, 30 Songdomirai-ro, Incheon 21990, Republic of Korea. *e-mail: jpkim153@dongguk.edu

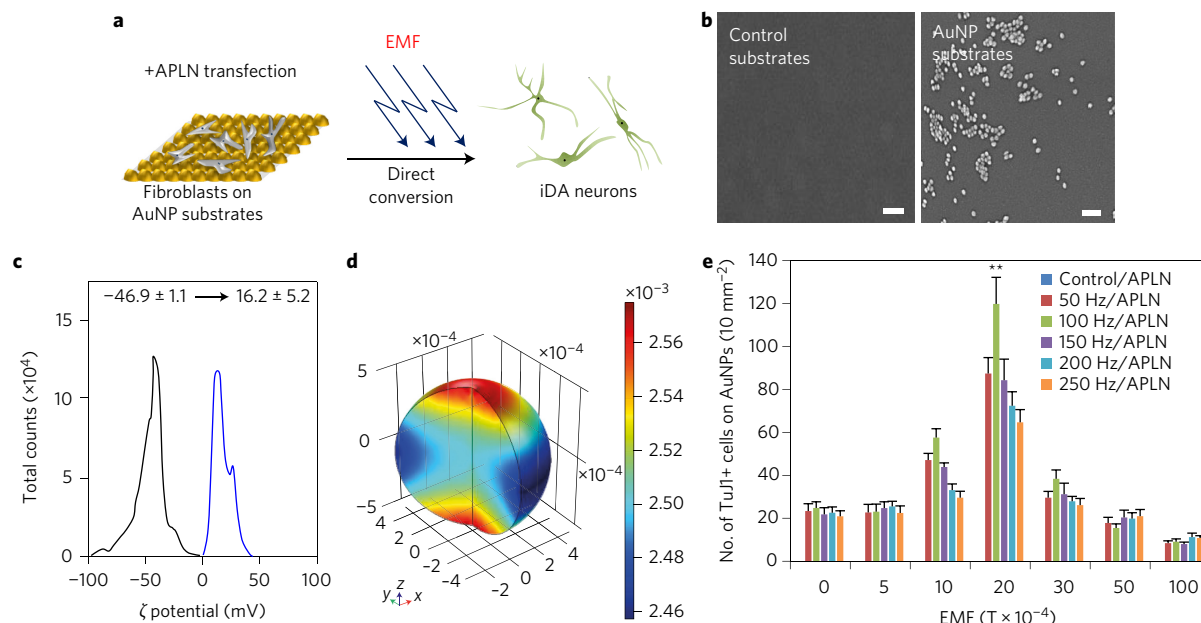


Figure 1 | EMF stimulation magnetizes AuNPs. **a**, Schematic illustrations showing the process for direct lineage reprogramming into iDA neurons using EMF-induced AuNP magnetization. Mouse fibroblasts transiently transfected with APLN were plated on the AuNP substrate and exposed to a specific frequency and intensity of EMF. **b**, SEM images of the control substrate and RGD–AuNP-coated substrate. Scale bars, 100 nm. **c**, The surface charge of citrate–AuNPs (black) and RGD–AuNPs (blue) was determined by zeta-potential measurement. The zeta potential of the AuNPs shifted from -46.9 ± 1.1 mV to 16.2 ± 5.2 mV on ligand exchange. **d**, Calculation of the magnetic flux spatial distribution on the surface of AuNPs during EMF exposure (100 Hz and 2×10^{-3} T). **e**, Number of TuJ1+ cells generated on magnetized AuNPs under different intensities and frequencies of EMF exposure. Data are represented as mean \pm s.e.m. ($n = 5$). ** $P < 0.01$, one way ANOVA.

and RGD peptides were introduced to increase biocompatibility and to facilitate cell-surface integrin binding to the AuNPs, respectively (Supplementary Fig. 1a). Modified AuNPs and RGD peptides were analysed by ultraviolet-visible (UV-vis) spectroscopy, dynamic light scattering (DLS), zeta-potential measurement, HPLC and electrospray ionization mass spectrometry (MS). The absorption maximum of the AuNPs shifted from 525 to 535 nm (Supplementary Fig. 1d), the average size of the particles increased from 23.3 ± 3.2 nm to 35.6 ± 8.8 nm (Supplementary Fig. 1e) and the surface charge of the AuNPs shifted from -46.9 ± 1.1 mV to 16.2 ± 5.2 mV as the thiol ligands were introduced (Fig. 1c and Supplementary Fig. 1b,c). These results show that the modified AuNPs are well dispersed in solution and can interact effectively with the negatively charged cell surface. Modified AuNPs were added to gelatine-coated glass coverslips to form culture substrates. Scanning electron microscope (SEM) analysis confirmed the surface binding of the AuNPs without a notable aggregation (Fig. 1b). Next, TTFs transiently transfected with plasmids that express the APLN factors were plated onto the AuNP substrates and exposed to EMF (Fig. 1a and Supplementary Fig. 1g,h).

We examined whether the EMF generator is capable of producing constant field intensities and frequencies within the cell-culture incubator. Monitoring EMF intensities with a Gauss meter confirmed that constant EMF intensities of different frequencies were generated at the centre area between the coils (Supplementary Fig. 1f,g). The AuNPs showed no magnetism in the absence of EMF (Supplementary Fig. 1l). We next calculated the distribution and gradient of the magnetic field on the EMF-exposed AuNP substrates. This revealed significant changes in the magnetic flux, which further confirmed the surface magnetization after EMF exposure (Fig. 1d).

To investigate how EMF exposure affects lineage reprogramming, APLN-transfected fibroblasts were exposed to a range of

EMF frequencies and intensities and the iDA lineage reprogramming was assessed. Exposure to a 2×10^{-3} T/100 Hz EMF significantly increased the generation of TuJ1-positive (TuJ1+) and Th-positive (Th+) iDA neurons without cytotoxicity (Fig. 1e and Supplementary Fig. 2a,b). Other EMF frequencies and/or intensities did not result in large differences in the number of TuJ1+ and Th+ cells relative to untreated controls (Fig. 1e and Supplementary Fig. 2a,b). The expression of mature neuronal markers was also highly increased in the 2×10^{-3} T/100 Hz EMF condition (Supplementary Fig. 2c). We confirmed that there were no differences in transfection efficiency between the control and the EMF-induced groups (Supplementary Fig. 1i-k).

Electromagnetized AuNPs mediate efficient direct lineage reprogramming. To explore the effects of EMF in more detail, we analysed the expression of multiple neuronal markers. Cultures exposed to a 2×10^{-3} T/100 Hz EMF exhibited an efficient iDA formation (Fig. 2a) with significant increases in the number of TuJ1+ and Map2+ iDA neurons relative to the controls (EMF or AuNP only) (Fig. 2b). Consistent with this result, expressions of the mature DA neuronal marker genes *TuJ1*, *Neurod1*, *Map2*, *Synapsin*, *Pitx3*, *Th*, *Dat* and *Vmat2* were significantly increased in EMF-exposed cultures (Fig. 2d and Supplementary Fig. 3c). The induction of gene expression was specific to the neuronal lineage, as the expression of genes characteristic of other lineages was not observed (Supplementary Fig. 2e).

We next assessed the efficiency of the EMF/AuNP-induced lineage conversion by measuring the proportion of cells that expressed the specific midbrain dopaminergic marker Pitx3 after EMF stimulation of the TTFs derived from *Pitx3-eGFP* knock-in (KI) mice¹². Transfection of the APLN factors alone resulted in ~3% GFP-positive (GFP+) iDA neurons (Fig. 2c). However, there was a near 20-fold increase in Pitx3-eGFP+ cells relative to the controls ten days after EMF exposure (Fig. 2c). We assessed the fidelity

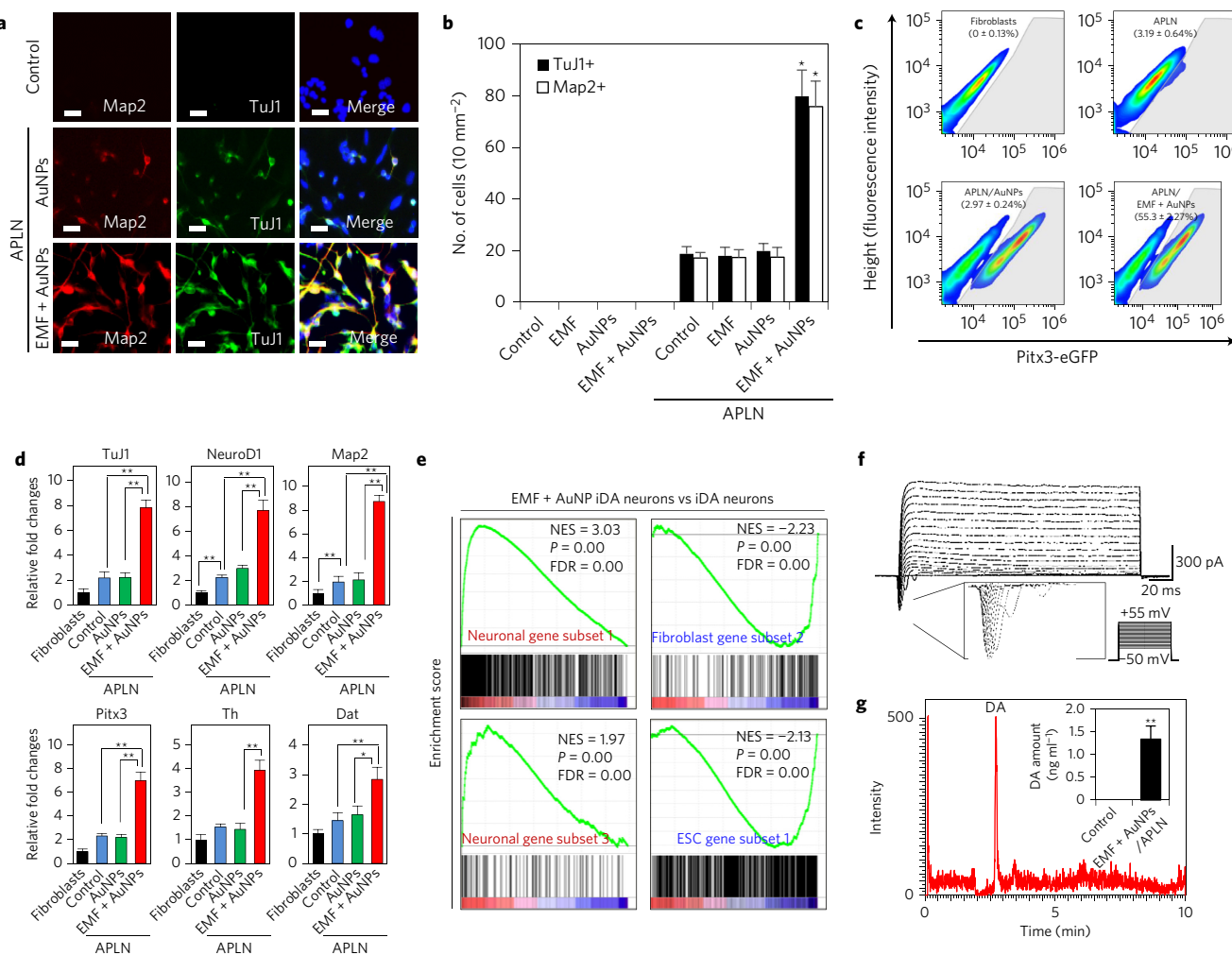


Figure 2 | Efficient direct lineage reprogramming of somatic fibroblasts into iDA neurons on EMF-induced magnetized AuNPs. **a**, Immunostaining for the mature neuronal markers MAP2 and TuJ1 on a control AuNP substrate and a magnetized AuNP substrate after exposure to $2 \times 10^{-3} \text{ T}/100 \text{ Hz}$ EMF. Scale bars, 50 μm . **b**, Numbers of TuJ1+ and Map2+ cells per field. Data are represented as mean \pm s.e.m. ($n = 5$ for each group). * $P < 0.05$, one-way ANOVA test. Three independent experiments with three replicates were performed. Ten independent visual fields per replicate were examined. **c**, FACS analysis of Pitx3-eGFP+ cells from Pitx3-eGFP KI fibroblasts in the control (untreated, top left), APLN (top right), APLN transiently transfected (bottom left) and APLN transiently transfected on EMF-induced magnetized AuNP substrate (APLN/AuNPs (bottom right)) conditions 10 d after transfection. **d**, qRT-PCR analysis of the DA neuronal markers at 10 d after transfection on EMF-induced magnetized AuNP substrates. Expression levels were normalized to GAPDH. Data are presented as mean \pm s.e.m., ANOVA, * $P < 0.05$, ** $P < 0.01$. **e**, CellNet-based GSEA of the global gene expression patterns of EMF-induced magnetized AuNPs versus control; gene sets of the GRNs in the CellNet database were used. P , nominal P value. **f**, Representative voltage-dependent membrane currents of iDA neurons generated by the magnetized AuNP condition. **g**, Representative DA measurement of KCl iDA release from EMF-induced iDA neurons by LC/MS analysis. Data represent mean \pm s.e.m., three independent experiments were performed.

of EMF-induced iDA (EMF-iDA) neuron conversion using CellNet analysis¹⁶. The gene regulatory networks (GRNs) for neurons, fibroblasts and embryonic stem (ES) cells from CellNet were compared with the gene expression profiles of EMF-iDA neurons using gene-set enrichment analysis (GSEA). Neuronal gene sets were enriched in EMF-iDA versus control iDA neurons, whereas fibroblast and ES cell gene sets were negatively enriched (Fig. 2e and Supplementary Table 1), which indicates that EMF-iDA neurons are globally more similar to endogenous DA neurons. Additionally, we examined the electrophysiological properties of EMF-iDA neurons using whole-cell patch clamping. Of the 12 cells examined from EMF-exposed cultures, 11 displayed evoked action potentials (Supplementary Fig. 2d) and fast inactivated inward and outward currents (Fig. 2f), consistent with mature neurons. In contrast, cells in the control APLN-transfected cultures did not exhibit fast inward Na currents (Supplementary Fig. 3a). Moreover, seven days after reprogramming, the mean input

resistance, average resting potential and action potential amplitude of the EMF-iDA neurons were similar to those of primary DA neurons (Supplementary Figs 2f and 3b). Additionally, EMF-iDA neurons exhibited dopamine (DA) release in response to a high-potassium-induced depolarization (Fig. 2g), consistent with DA neuron function.

The robust APLN-driven lineage reprogramming promoted by EMF/AuNPs led us to examine whether EMF/AuNP conditions can mediate lineage conversion with fewer reprogramming factors or small-molecule substitutes. As Ascl1 alone is sufficient to generate induced neurons¹⁷, we cultured fibroblasts that expressed Ascl1 alone or with small molecules with pro-neurogenic properties, including CHIR99021, Forskolin and valproic acid (CFV)^{18–20} in the presence of EMF/AuNP. Indeed, Ascl1-transfected fibroblasts exposed to EMF/AuNP conditions efficiently generated iDAs (Supplementary Fig. 3d,f). In addition, CFV treatment also yielded TuJ1+ and Map2+ iDAs 15 days after exposure to EMF/AuNP

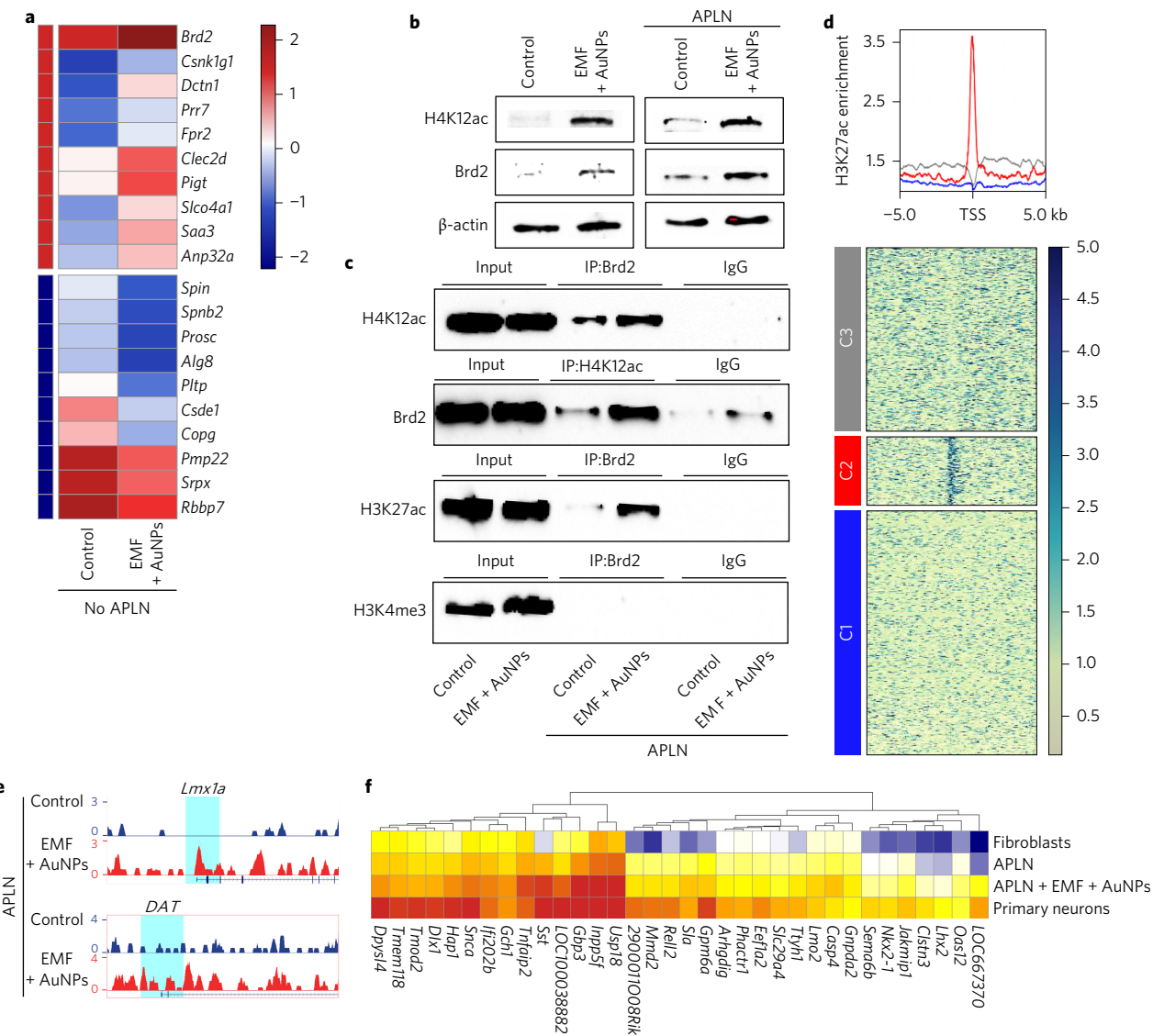


Figure 3 | Molecular mechanisms of direct lineage reprogramming by EMF-induced magnetized AuNPs. **a**, Heat map that represents the global gene-expression pattern of transcription factors in control fibroblasts and the fibroblasts grown on magnetized AuNPs with EMF exposure. **b**, Western blot analysis of H4K12ac and Brd2 in control fibroblasts and the EMF-exposed fibroblasts with and without the reprogramming factors, APLN. **c**, Co-immunoprecipitation (IP) of H4K12ac, Brd2, H3K27ac and H3K4me3 complexes in lysates prepared from the control and EMF-exposed fibroblasts 10 d after reprogramming the factor transfection. IgG, immunoglobulin. **d**, Heat maps that depict the genome-wide tag density of H3K27ac in EMF-AuNP-treated reprogramming. The H3K27ac coverage of TSSs for genes that contain ChIP peaks (top). The three divisions of the plots reflect the k-means clustering ($k = 3$). kb, kilobase pair. **e**, Genome browser track showing H3K27ac occupancy near the TSS of the neuronal genes *Lmx1a* and *DAT*. **f**, Heat map that shows the expression patterns of genes, which are both upregulated and H3K27ac occupied (C2) by EMF exposure.

conditions (Supplementary Figs 3e,f and 4a–d). No TuJ1+ or Map2+ cells were observed in the absence of EMF/AuNP conditions (Supplementary Fig. 4a,b). Thus, EMF-induced magnetized AuNPs can substitute for several reprogramming factors and can facilitate neuronal lineage conversion with minimal exogenous factors.

Mechanisms of electromagnetized AuNP-induced direct lineage reprogramming. To investigate the mechanisms by which EMF promotes lineage reprogramming, we analysed changes to the transcriptome of fibroblasts exposed to EMF/AuNP conditions (Fig. 3a). Expression levels of only 76 genes changed significantly, and among the most strongly upregulated was *Brd2*, which encodes the chromatin-modifying bromodomain-containing protein-2 (Fig. 3a). As *Brd2* is a key regulator of histone acetylation²¹, we assessed the expression of histone acetylation

complex constituents and *Brd2*-binding partners, which include *Smarca2*, *Gcn5* and *Tata-box binding protein*. All of these genes were upregulated in response to EMF/AuNP exposure (Supplementary Fig. 5a), as were histone H4 lysine 12 (H4K12) acetylation levels relative to untreated cultures (Fig. 3b and Supplementary Fig. 5b). Consistent with this, immunostaining confirmed the accumulation of *Brd2* and H3K27 acetylation in the presence of APLN transfection and EMF/AuNP exposure, whereas levels of methylated (me) H3K4me3 were unaffected (Supplementary Fig. 5b–d). Moreover, we found increased interactions between *Brd2* and both acetylated H3K27 and H4K12 in response to EMF/AuNP exposure by co-immunoprecipitation, whereas no interaction was detected between *Brd2* and H3K4me3 (Fig. 3c). This indicates that the increased histone acetylation is a specific effect of the EMF stimulation of the AuNPs.

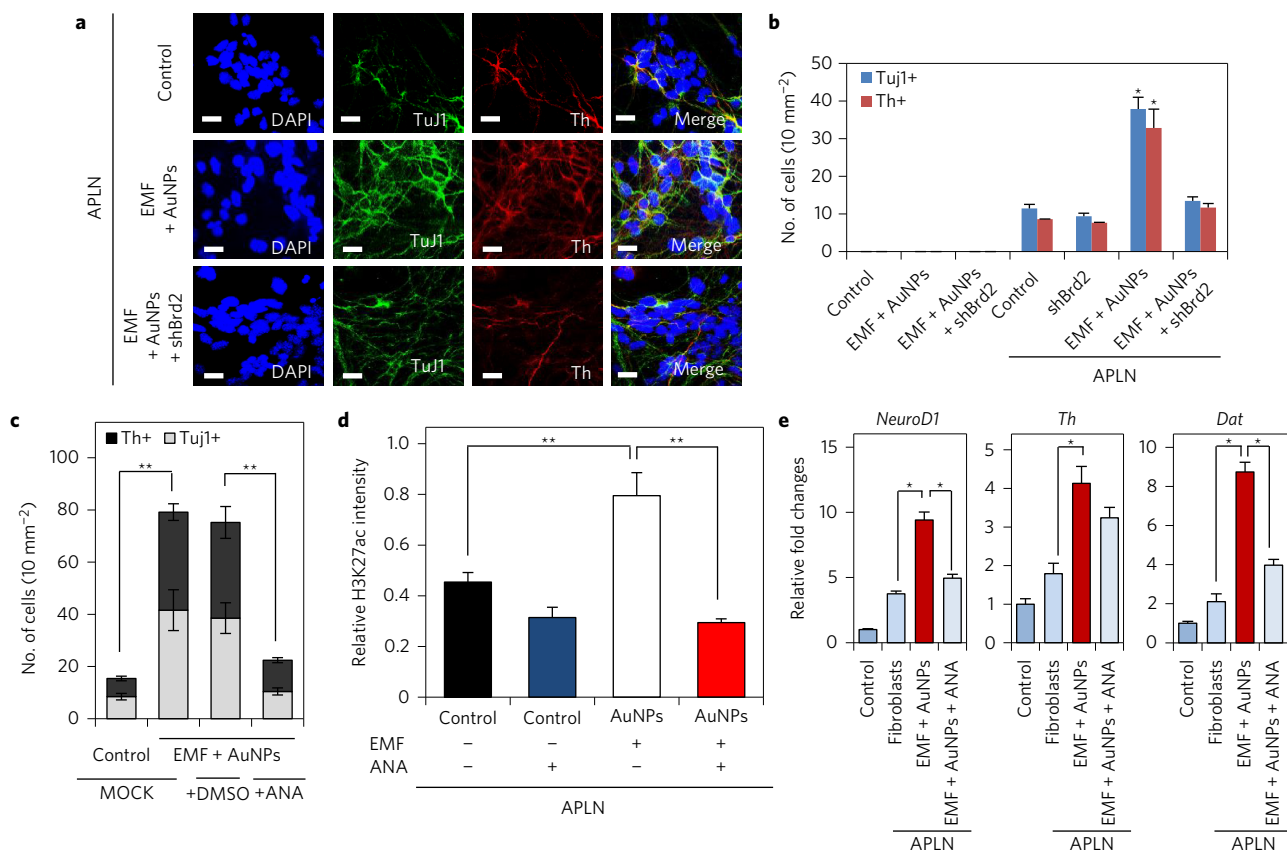


Figure 4 | Histone acetylation mediates EMF-induced efficient direct lineage reprogramming. **a**, Immunofluorescence staining of iDA neurons generated on EMF-exposed AuNP substrates in Brd2 knockdown fibroblasts. Cells were stained for the dopaminergic neuronal markers TuJ1 and Th at 10 d after APLN factor transfection. Scale bars, 50 μ m. DAPI, 2-(4-amidinophenyl)-1H-indole-6-carboxamide. **b**, Numbers of TuJ1 and Th + iDA neurons with and without Brd2 knockdown. Three independent experiments were performed. Data are presented as mean \pm s.e.m., ANOVA test, * P < 0.05. **c**, Numbers of TuJ1+ and TH+ cells in EMF cultures with and without ANA treatment. Data are presented as mean \pm s.e.m., Student's *t*-test, ** P < 0.01. DMSO, dimethylsulfoxide. MOCK refers to –DMSO, –ANA. **d**, Quantification of H3K27ac immunofluorescence intensities in the presence or absence of ANA 10 d after APLN transfection. Data are presented as mean \pm s.e.m., Student's *t*-test, ** P < 0.01. **e**, qRT-PCR analysis of the endogenous dopaminergic neuron markers *NeuroD1*, *Th* and *Dat* 10 d after APLN transfection and ANA treatment. Expression levels are normalized to GAPDH. Data are presented as mean \pm s.e.m., Student's *t*-test, * P < 0.05.

Additionally, we examined changes to the expression of other genes that encode chromatin-modifying proteins in the presence of magnetized AuNPs (Supplementary Fig. 5e) and confirmed that the effects of EMF/AuNP exposure were highly specific to *Brd2*.

We next examined how the EMF energy alters histone acetylation at neuronal gene promoters. Chromatin immunoprecipitation (ChIP) with antibodies that target H3K27ac (ac, acetyl) followed by sequencing (ChIP-seq) of APLN-expressing fibroblasts exposed to EMF/AuNP identified 2,646 genomic regions (collectively termed C2) occupied by H3K27ac with a high confidence at transcriptional start sites (TSSs) (Fig. 3d). Relative to untreated controls, 7,837 genomic regions (termed C1) lost H3K27ac deposition, and a third group, C3 (6,213 genomic regions), lacked H3K27ac specifically at TSSs. Moreover, we found that genes in C2 that harboured H3K27ac at their TSS were upregulated during the EMF-induced reprogramming relative to genes in C1 or C3 (Supplementary Fig. 6a,d). We confirmed that upregulated C2 genes were primarily neuron specific (Fig. 3f and Supplementary Fig. 6b,c), and gene ontology analysis confirmed that EMF-induced/H3K27ac-occupied C2 genes were primarily enriched in functions associated with ‘histone acetylation’ and ‘neurons’ (Supplementary Fig. 6e–g). Consistent with this, we observed that EMF exposure increased H3K27 acetylation at TSS regions of the neuronal genes *Lmx1a*, *NeuroD1*, *DAT*, *NeuN*, *Nf1*, *Med12* and *Hpn* (Fig. 3e and Supplementary Fig. 6h,i). ChIP-quantitative PCR (qPCR)

confirmed that the TSS of the *TH* gene is also enriched in H4K12ac in the EMF/AuNP-exposed cultures (Supplementary Fig. 6j). Taken together, these data support a model in which EMF/AuNP exposure promotes histone acetylation through *Brd2*, and thereby increases the accessibility of neuronal loci to APLN factors to enhance the reprogramming into iDA neurons.

To determine whether increased histone acetylation is functionally important for magnetized AuNP-induced reprogramming, we inhibited *Brd2* in EMF/AuNP-exposed cultures. Indeed, *Brd2* knockdown led to a significant decrease in iDA generation from fibroblasts subjected to EMF/AuNP-induced reprogramming, whereas *Brd2* suppression had no effect on basal iDA-neuron generation in response to APLN factor expression alone (Fig. 4a,b and Supplementary Figs 7a and 8a,b). Moreover, the expression of neuronal genes and the histone-acetylation levels were significantly decreased in response to *Brd2* knockdown in EMF/AuNP-exposed cultures that underwent either APLN- or CFV-mediated reprogramming (Supplementary Figs 7c,d and 8c,f–k). Furthermore, we observed that *Brd2* knockdown attenuated the H3K27ac accumulation at the endogenous *Th* promoter in cells subjected to EMF/AuNP-mediated APLN reprogramming (Supplementary Fig. 7e). Additionally, pharmacological suppression of HAT activity with anacardic acid (ANA) significantly suppressed the reprogramming efficiency, as evidenced by decreased numbers of iDA neurons and the

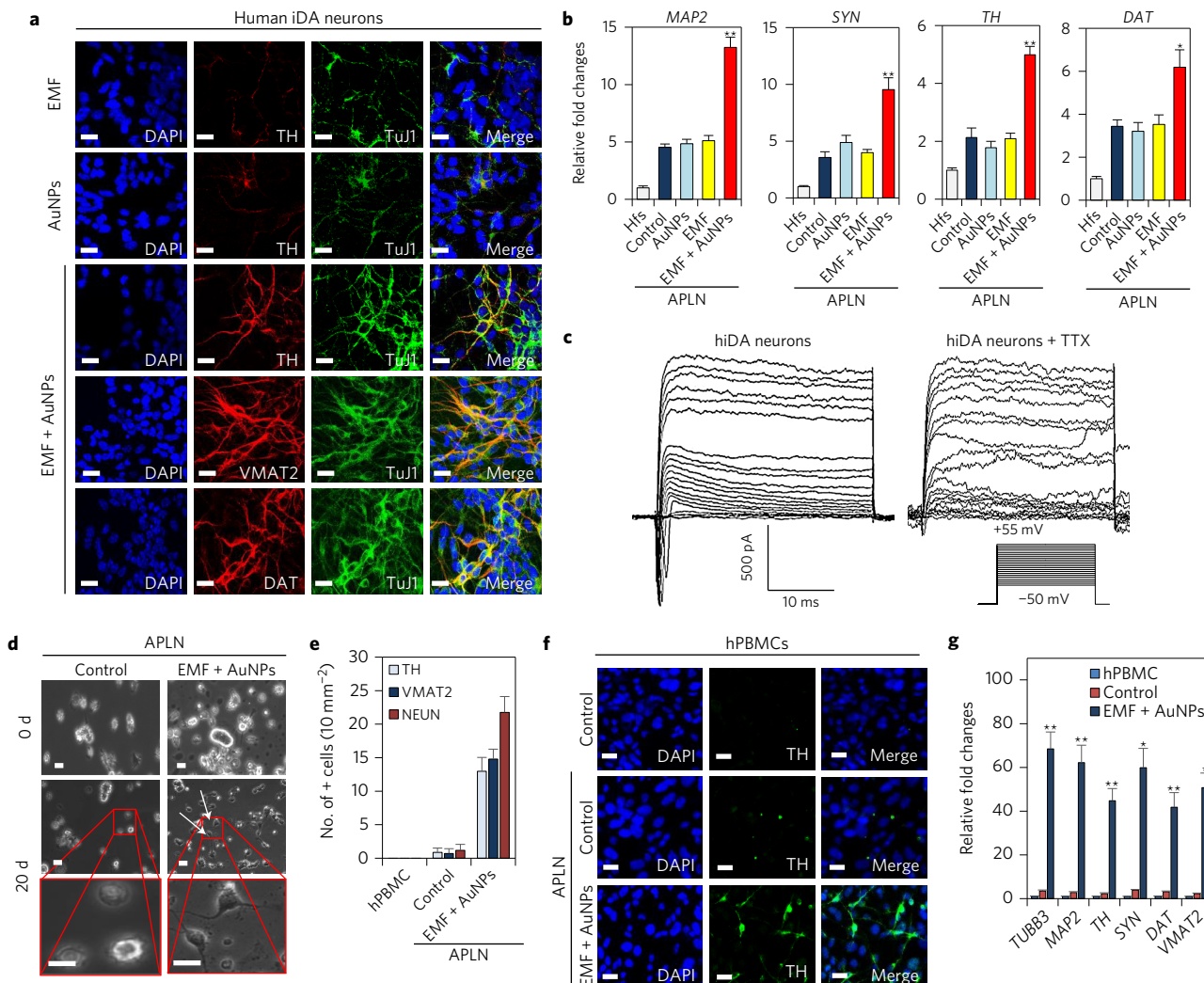


Figure 5 | Efficient direct lineage reprogramming of human cells into iDA neurons on EMF-induced magnetized AuNPs. **a**, Immunostaining analysis of DA neuronal markers TUJ1, TH, VMAT2 and DAT in EMF-derived hiDA neurons (human fibroblasts 52 years old, healthy control). Scale bars, 50 μ m. **b**, qRT-PCR analysis of the DA neuronal markers MAP2, SYNAPSIN, TH and DAT at 10 d after APLN transfection. Three independent experiments were performed; expression levels are normalized to GAPDH. Data are presented as mean \pm s.e.m., ANOVA test, * P < 0.05, ** P < 0.01. **c**, Representative traces show the presence of voltage-dependent Na⁺ and K⁺ currents in EMF-induced hiDA neurons. Left panel: iDA neuron before TTX application. Right panel: same neuron after treatment with TTX. **d**, Phase-contrast images of hPBMCs (female, 19 years old, healthy control) at 0 d (top images) and 20 d after reprogramming factor infection (lower images). Scale bars, 25 μ m. **e**, Number of positive cells of human-blood-derived hiDA neuron markers, TH, VMAT2 and NeuN, at 20 d after APLN-factor infection. Three independent experiments were performed; the data represent the mean \pm s.e.m. **f**, Immunofluorescence images of human-blood-derived hiDA neurons stained with the DA neuron marker TH. iDA neurons were derived from hPBMCs for 20 d after factor infection. Scale bars, 20 μ m. **g**, qRT-PCR analysis of DA neuronal markers TUBB3, MAP2, TH, SYNAPSIN, DAT and VMAT2 in hiDA neurons at 20 d after direct conversion under the magnetized AuNP condition. Three independent experiments were performed. Data are presented as mean \pm s.e.m., ANOVA test, * P < 0.05, ** P < 0.01.

reduced expression of DA neuronal markers in cultures that underwent EMF/AuNP-mediated reprogramming (Fig. 4c,e and Supplementary Figs 7f and 8d,e). However, ANA treatment did not significantly affect *Th* expression (Fig. 4e), which possibly suggests the incomplete inhibition of HAT activity by ANA, or more-complex, non-catalytic roles of Brd2 in regulating the *Th* locus. We also observed that H3K27ac and H4K12ac were reduced by ANA treatment (Fig. 4d and Supplementary Fig. 7b). These findings provide strong evidence for a model whereby the EMF induction of AuNPs promotes iDA reprogramming by promoting histone acetylation and gene expression at neuronal loci.

Electromagnetized AuNPs induced efficient direct lineage reprogramming of human cells. The efficient EMF/AuNP-

mediated lineage reprogramming of mouse somatic cells prompted us to examine whether our findings extended to human cells. APLN-transfected human fibroblasts were plated on the AuNP substrates and exposed to 2×10^{-3} T/100 Hz of EMF. Two weeks after EMF exposure, increases in TH-, VMAT2- and DAT-positive iDA neurons were observed (Fig. 5a and Supplementary Fig. 9a). Endogenous MAP2, SYN, TH and DAT were also significantly upregulated by the EMF/AuNP-exposed cultures (Fig. 5b). As with murine cells, EMF/AuNP-induced human iDA (EMF-hiDA) neurons showed functional electrophysiological properties and evoked action potentials (Supplementary Fig. 10a,b). These included fast inactivated inward and outward currents characteristic of voltage-dependent Na⁺ and K⁺ currents and inward Na currents that were blocked by tetrodotoxin (TTX) administration (Fig. 5c). Further, we verified that EMF-hiDA

neurons contained intracellular DA that was released into the medium on 50 mM KCl stimulation (Supplementary Fig. 9f), consistent with the functional properties of midbrain DA neurons. Additionally, BRD2 was highly upregulated in EMF-hiDA cultures (Supplementary Fig. 10d), and the knockdown of BRD2 abrogated hiDA reprogramming (Supplementary Figs 9b–e and 10c). We confirmed that H3K27ac and H4K12ac levels decreased on BRD2 knockdown in EMF/AuNP-treated cultures (Supplementary Figs 9e and 10e). Thus, both mouse and human somatic cells are amenable to EMF/AuNP-induced iDA conversion.

Given the dramatic increase in iDA-generation efficiency with the EMF/AuNP system, we tested whether readily accessible human peripheral mononuclear blood cells (PBMCs) could be reprogrammed. PBMCs were transduced with lentiviral vectors that encoded the APLN factors and were exposed to EMF/AuNPs. Remarkably, ten days after transduction, the PBMC-derived EMF-hiDA neurons acquired a mature neuronal morphology, which included dendritic spine-like protrusions, only in the presence of EMF/AuNPs (Fig. 5d). PBMC-derived hiDA neurons activated TH, VMAT2, TUBB3, SYN, DAT and NEUN in EMF/AuNP conditions (Fig. 5e–g and Supplementary Fig. 11a,b). These cells produced DA and downregulated haematogenic gene expression (Supplementary Fig. 11c,d), and thus PBMCs are a viable cell source for hiDA generation.

Electromagnetized AuNPs induced *in vivo* direct lineage reprogramming. We next asked whether EMF/AuNP exposure can promote lineage reprogramming *in vivo*. To this end, we established a 1-methyl-4-phenyl-1,2,3,6-tetrahydropyridine (MPTP)-induced PD mouse model. Along with APLN lentiviral particles, AuNPs were implanted in solution into the striatum of MPTP-treated mice (Fig. 6a). These animals were then exposed to EMF for three hours per day for the next four weeks (Supplementary Fig. 12a).

First, we examined motor function in these experimental mice relative to controls. Strikingly, EMF-exposed MPTP mice exhibited a remarkable restoration of movement in open-field tests relative to control groups, including increased total distance travelled and a higher percentage of total activity in the centre zone of the open field (Fig. 6b and Supplementary Fig. 12c). Additionally, the EMF-treated group exhibited a significant increase in rearing behaviour compared with controls (Supplementary Figs 12c and 13a,e). To assess directly the effects of EMF on the lineage reprogramming of DA neurons *in vivo*, we performed 3,3'-diaminobenzidine (DAB) staining using a TH antibody in the mouse striatum (Fig. 6c and Supplementary Fig. 13b). EMF exposure significantly increased the numbers of TH+ cells relative to those of MPTP-treated controls (Supplementary Fig. 12b). More Map2-, Tuj1-, TH-, Vmat2- and Pitx3-positive cells also responded to EMF exposure (Supplementary Fig. 13c). Similarly, quantitative reverse transcription (qRT)-PCR showed an increased expression of *Vmat2*, *Th*, *Map2* and *Dat* in EMF-treated MPTP mice relative to controls (MPTP alone, or MPTP and APLN factors (Supplementary Fig. 13d)).

Next, we performed slice recordings to evaluate the electrophysiological activities of *in vivo* converted iDA neurons. Importantly, synapsin-GFP+ *in vivo* converted neurons showed fast inward sodium currents and outward potassium currents that were completely abolished by TTX administration, which indicates the presence of well-developed voltage-gated Na⁺ and K⁺ channels (Fig. 6d and Supplementary Fig. 13f). Moreover, we recorded spontaneous excitatory postsynaptic currents (EPSCs) in GFP+ iDA neurons, and these synaptic activities were efficiently blocked by CNQX (6-cyano-7-nitroquinoxaline-2,3-dione) and AP5 (2-amino-5-phosphonopentanoic acid), which suggests that iDA neurons reprogrammed with electromagnetized formed functional synapses with other neurons (Fig. 6e).

Additionally, we assessed the efficacy of EMF/AuNP-mediated iDA conversion for reversing phenotypes in a second PD model in which one hemisphere of the midbrain is lesioned with 6-hydroxydopamine (6-OHDA). After three weeks of 6-OHDA treatment, a solution of AuNPs and APLN lentiviral particles was injected into the striatum, as in the MPTP model. These 6-OHDA mice were then exposed to EMF for three hours per day for eight weeks after transplantation. Remarkably, EMF exposure combined with APLN factors led to a significant reduction in apomorphine-induced rotation relative to controls (Supplementary Figs 12d and 13g). Moreover, 6-OHDA mice exposed to EMF/AuNPs exhibited larger numbers of Dat+ and Th+ iDA neurons in the striatum (Supplementary Figs 12e,f and 13h). Additionally, we confirmed the electrophysiological properties and elevated DA levels in the EMF/AuNP-treated striatum of 6-OHDA-lesioned murine neurons (Fig. 6f), which demonstrates the formation of synapses with other neurons within the host brain.

Finally, to test whether iDA neurons were reprogrammed from astrocytes *in vivo*, we used genetic lineage tracing to track the origin of the iDA neurons. To this end, glial fibrillary acidic protein (GFAP)-Cre transgenic mice were injected with the flip-excision (FLEx) tracer reporter (FLEx-synapsin:GFP) along with lentiviral APLN particles and AuNPs. GFAP-Cre is specifically expressed in astrocytes, and thus the FLEx-synapsin:GFP reporter will only be expressed in iDA neurons derived from astrocytes²². These mice were then exposed to EMF. Eight weeks after conversion, the number of GFP+ cells was quantified. No GFP+ cells were observed in controls lacking APLN. In contrast, we observed a significant increase in GFP+ reprogrammed cells on EMF exposure (Fig. 6h). Reprogrammed GFP+ cells were positive for Th, Dat, Vmat2, Nurr1 and Pitx3, which demonstrates directly that EMF-exposed AuNPs along with APLN factors convert astrocytes into iDA neurons in the brain (Fig. 6g-i and Supplementary Fig. 13i).

Taken together, these results demonstrate that EMF exposure in the presence of AuNPs and the APLN reprogramming factors can dramatically improve the efficiency of *in vivo* lineage reprogramming, which in turn can rescue Parkinsonian phenotypes in mouse models of PD.

Discussion

EMFs can influence cell migration, differentiation, apoptosis and the stress response^{3,23–25}. We previously demonstrated that specific EMF frequencies can alter cell fate and activate gene-transcription networks essential for the epigenetic reprogramming to pluripotency²⁶. These results led us to examine whether EMF can improve the reprogramming efficiency of somatic cells into neurons. Indeed, a specific frequency and intensity of EMF stimulation conveyed via magnetized AuNPs dramatically enhanced the efficacy of direct lineage reprogramming into iDA neurons in the presence of transient reprogramming transcription-factor expression *in vitro*. Although many other methods, including the application of small molecules, have been reported to facilitate efficient and safe direct lineage reprogramming, we propose that EMF may be particularly advantageous owing to its high efficiency, low toxicity, ease of preparation and controllability. Our results suggest that EMF-exposed AuNPs facilitate conversion into the neuronal lineage by promoting chromatin remodelling and enabling the transcriptional changes necessary for the reprogramming process. Thus, somatic cell reprogramming using magnetized AuNPs may represent a viable therapeutic strategy to replace neurons lost in neurodegenerative diseases.

Importantly, we demonstrate the safe and efficient iDA lineage reprogramming *in vivo* using murine PD models. Such *in vivo* lineage-reprogramming therapies have been attempted in various human disease models^{27–29}. However, the generation of new functional cells from resident somatic cells was inefficient and the reprogrammed

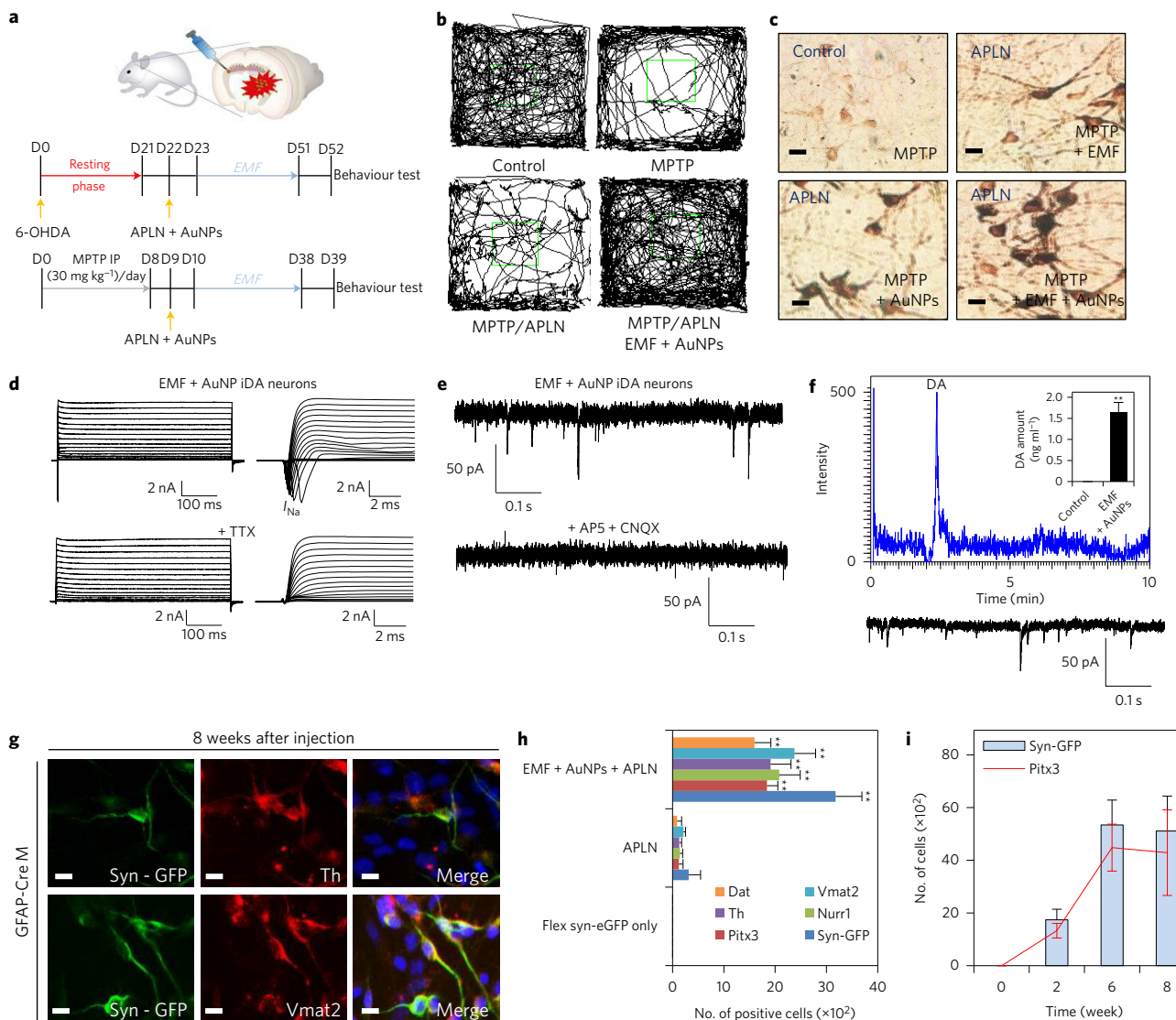


Figure 6 | Rescue of Parkinsonian phenotypes in MPTP- and 6-OHDA-induced PD mouse models by *in vivo* direct lineage reprogramming using the EMF-induced magnetized AuNP system. **a**, A schematic diagram of *in vivo* direct lineage reprogramming using EMF-induced magnetized AuNPs in a MPTP- or 6-OHDA-induced PD mouse model. **b**, Track sheets show the alteration in the locomotion in the MPTP mouse model (control, MPTP, MPTP + APLN and MPTP + APLN + EMF + AuNPs). For the MPTP-induced PD mice, we observed a shorter travelling distance to the centre zone, whereas increased ambulation distances were observed in the EMF + AuNP-treated MPTP-induced PD mouse model. **c**, Representative image of the DAB-TH staining of EMF-induced iDA neurons in the striatum from the control, EMF only, AuNPs only and EMF + AuNPs groups. Scale bars, 30 µm. **d**, Representative voltage-dependent membrane currents show fast inward sodium currents and slow outward potassium currents of GFP+ iDA neurons in the MPTP-treated mouse striatum (top panel). The same neuron after treatment with TTX (bottom panel) with EMF + AuNPs. **e**, Example of the spontaneous postsynaptic activity recorded from EMF-induced iDA neurons (top panel). These postsynaptic events were blocked by CNQX (AMPA glutamate receptor antagonist) and AP5 (NMDA glutamate receptor antagonist) (bottom panel). **f**, DA measurement of iDA neurons in the striatum of 6-OHDA-lesioned mice and EMF-AuNP-treated 6-OHDA-lesioned mice ($n=3$ per group) (top). Data are presented as means \pm s.e.m., Student's t-test, ** $P < 0.01$. An example of spontaneous postsynaptic currents of GFP+ *in vivo* converted iDA neurons in the EMF-treated 6-OHDA-lesioned striatum (bottom). **g**, Immunostaining of Th and Vmat2 in EMF-induced *in vivo* converted iDA neurons at 8 weeks. Scale bars, 40 µm. **h**, Quantification of positive cells from **g** ($n=7$ mice for each group). Data are presented as mean \pm s.e.m., Student's t-test, ** $P < 0.01$. **i**, Number of EMF-induced *in vivo* converted GFP+ iDA neurons at 2 weeks, 6 weeks and 8 weeks after AuNP injection.

cells did not adequately reproduce the original functional cells^{27,28,30,31}. In the present study, the EMF-magnetized AuNP system facilitates a high conversion rate from somatic cells and the resulting iDA neurons exhibit many functional characteristics of midbrain DA neurons. In this respect, our system overcomes prior obstacles to *in vivo* application. The EMF system represents a non-invasive method to potentiate *in vivo* direct reprogramming into neurons and thus may be more suitable for clinical application. Taken together, our findings suggest that the reprogramming of somatic cells into

neurons by electromagnetized AuNPs may offer a new therapeutic approach for PD and other neurodegenerative diseases.

Methods

Methods and any associated references are available in the online version of the paper.

Received 6 August 2016; accepted 9 June 2017;
published online 17 July 2017

References

- Golbach, L. A. *et al.* Calcium homeostasis and low-frequency magnetic and electric field exposure: a systematic review and meta-analysis of *in vitro* studies. *Environ. Int.* **92–93**, 695–706 (2016).
- National Institute of Environmental Health Sciences and National Institutes of Health *EMF Electric and Magnetic Fields Associated with the Use of Electric Power* (NIEHS/DOE EMF Rapid Program, 2002).
- Lester, G., Aaron, R. K., Neame, P. & Caterson, B. Low frequency EMF regulates chondrocyte differentiation and expression of matrix proteins. *J. Orthop. Res.* **20**, 40–50 (2002).
- De Mattei, M. *et al.* Effects of electromagnetic fields on proteoglycan metabolism of bovine articular cartilage explants. *Connect. Tissue Res.* **44**, 154–159 (2003).
- Funk, R. H., Monsees, T. & Özkur, N. Electromagnetic effects—from cell biology to medicine. *Prog. Histochem. Cytochem.* **43**, 177–264 (2009).
- Cho, H. *et al.* Neural stimulation on human bone marrow-derived mesenchymal stem cells by extremely low frequency electromagnetic fields. *Biotechnol. Prog.* **28**, 1329–1335 (2012).
- Seong, Y., Moon, J. & Kim, J. Egr1 mediated the neuronal differentiation induced by extremely low-frequency electromagnetic fields. *Life Sci.* **102**, 16–27 (2014).
- Motohashi, T. *et al.* Gene array analysis of neural crest cells identifies transcription factors necessary for direct conversion of embryonic fibroblasts into neural crest cells. *Biol. Open* **5**, 311–322 (2016).
- Vierbuchen, T. *et al.* Direct conversion of fibroblasts to functional neurons by defined factors. *Nature* **463**, 1035–1041 (2010).
- Marro, S. *et al.* Direct lineage conversion of terminally differentiated hepatocytes to functional neurons. *Cell Stem Cell* **9**, 374–382 (2011).
- Ieda, M. *et al.* Direct reprogramming of fibroblasts into functional cardiomyocytes by defined factors. *Cell* **142**, 375–386 (2010).
- Kim, J. *et al.* Functional integration of dopaminergic neurons directly converted from mouse fibroblasts. *Cell Stem Cell* **9**, 413–419 (2011).
- Torper, O. *et al.* Generation of induced neurons via direct conversion *in vivo*. *Proc. Natl Acad. Sci. USA* **110**, 7038–7043 (2013).
- Guo, Z. *et al.* *In vivo* direct reprogramming of reactive glial cells into functional neurons after brain injury and in an Alzheimer's disease model. *Cell Stem Cell* **14**, 188–202 (2014).
- Salata, O. V. Applications of nanoparticles in biology and medicine. *J. Nanobiotechnol.* **2**, 3 (2004).
- Morris, S. A. *et al.* Dissecting engineered cell types and enhancing cell fate conversion via CellNet. *Cell* **158**, 889–902 (2014).
- Chanda, S. *et al.* Generation of induced neuronal cells by the single reprogramming factor ASCL1. *Stem Cell Rep.* **3**, 282–296 (2014).
- Hu, W. *et al.* Direct conversion of normal and Alzheimer's disease human fibroblasts into neuronal cells by small molecules. *Cell Stem Cell* **17**, 204–212 (2015).
- Li, X. *et al.* Small-molecule-driven direct reprogramming of mouse fibroblasts into functional neurons. *Cell Stem Cell* **17**, 195–203 (2015).
- Hei, W. H. *et al.* Schwann-like cells differentiated from human dental pulp stem cells combined with a pulsed electromagnetic field can improve peripheral nerve regeneration. *Bioelectromagnetics* **37**, 163–174 (2016).
- LeRoy, G., Rickards, B. & Flint, S. The double bromodomain proteins Brd2 and Brd3 couple histone acetylation to transcription. *Mol. Cell* **30**, 51–60 (2008).
- Torper, O. *et al.* *In vivo* reprogramming of striatal NG2 glia into functional neurons that integrate into local host circuitry. *Cell Rep.* **12**, 474–481.
- Delle Monache, S., Alessandro, R., Iorio, R., Gualtieri, G. & Colonna, R. Extremely low frequency electromagnetic fields (ELF-EMFs) induce *in vitro* angiogenesis process in human endothelial cells. *Bioelectromagnetics* **29**, 640–648 (2008).
- Simko, M., Kriehuber, R., Weiss, D. & Luben, R. Effects of 50 Hz EMF exposure on micronucleus formation and apoptosis in transformed and nontransformed human cell lines. *Bioelectromagnetics* **19**, 85–91 (1998).
- Blank, M. & Goodman, R. Electromagnetic fields stress living cells. *Pathophysiology* **16**, 71–78 (2009).
- Baek, S. *et al.* Electromagnetic fields mediate efficient cell reprogramming into a pluripotent state. *ACS Nano* **8**, 10125–10138 (2014).
- Qian, L. *et al.* *In vivo* reprogramming of murine cardiac fibroblasts into induced cardiomyocytes. *Nature* **485**, 593–598 (2012).
- Song, K. *et al.* Heart repair by reprogramming non-myocytes with cardiac transcription factors. *Nature* **485**, 599–604 (2012).
- Rivetti di Val Cervo, P. *et al.* Induction of functional dopamine neurons from human astrocytes *in vitro* and mouse astrocytes in a Parkinson's disease model. *Nat. Biotechnol.* **35**, 444–452 (2017).
- Muraoka, N. & Ieda, M. Direct reprogramming of fibroblasts into myocytes to reverse fibrosis. *Ann. Rev. Physiol.* **76**, 21–37 (2014).
- Chen, J. X., Plonowska, K. & Wu, S. M. Somatic cell reprogramming into cardiovascular lineages. *J. Cardiovasc. Pharmacol. Ther.* **19**, 340–349 (2014).

Acknowledgements

This work was supported by the National Research Foundation of Korea funded by the Ministry of Education, Science, and Technology (NRF-2017M3A9C6029306, 2016R1A2B2014195, 2013M3A9B4076483, NRF-2015 M3A9B4051064), Korea Health Technology R&D Project, Ministry of Health & Welfare (HI16C1176), the Next-Generation BioGreen 21 Program, Rural Development Administration (PJ011077) and the Ministry of Food and Drug Safety in 2017 (14172MFDS974).

Author contributions

J.Y., Y.K. and J.K. designed the study. J.Y., E.L., H.Y.K., D.Y., J.J., H.K., Y.C., W.L., J.S., S.B., W.Jang, W.Jun, S.K., J.H. and H.P. performed the experiments. J.Y., J.K. and C.J.L. analysed the data. Y.K., E.L., H.Y.K., D.Y. and S.H.M. contributed materials and/or analysis tools. The manuscript was written based on contributions by all the authors. All the authors approved the final version of the manuscript.

Additional information

Supplementary information is available in the [online version of the paper](#). Reprints and permissions information is available online at [www.nature.com/reprints](#). Publisher's note: Springer Nature remains neutral with regard to jurisdictional claims in published maps and institutional affiliations. Correspondence and requests for materials should be addressed to J.K.

Competing financial interests

The authors declare no competing financial interests.

Methods

EMF exposure. We constructed an EMF-generation system as described previously^{6,32,33}. The system consisted of an a.c. power supply (PCR-100L, Kikusui), a pulsed EMF (PEMF)-waveform generator and a Helmholtz coil. We used the COMSOL 3.4 Multiphysics Unit (COMSOL) to design a Helmholtz coil. A Helmholtz coil consists of two identical circular magnetic coils (Supplementary Figs 1h and 12a) and produces a region of nearly uniform magnetic field. The circular magnetic coil was of diameter 70 cm and width 10 cm, and the distance between two coils was 35 cm for *in vivo* EMF exposure, whereas its inner diameter, width and distance were 22, 6 and 11 cm for *in vitro* EMF exposure. Both coils consisted of 1,000 turns of enamel copper wire (AWG no. 25, 0.5 mm diameter) with an acrylic tube (Supplementary Figs 1h and 12a). The waveform of the PEMF was generated by a microcontroller (Atmega328P, Atmel) and confirmed by an oscilloscope (TDS3032, Tektronix). The EMF waveform had a repetitive rate of 50, 100, 150, 200 and 250 Hz. The magnetic field intensity was theoretically expressed by: $B = (8.99178 \times 10^{-7})NI/R^2 T$, where I is the current through the coils, N is the number of turns of each coil and R is the radius of the coils. The waveform and intensity of the magnetic field produced by each stimulator unit was confirmed with an oscilloscope and Gauss meter (TM-701, Kanetec), respectively (Supplementary Fig. 1fg). Cell-culture dishes (*in vitro*) and a mouse-containing box (*in vivo*) were placed in the middle of the plane between two coils. One pair of Helmholtz coils was used both for the control and sham exposure and without a PEMF signal generator. To exclude the uncontrolled thermal effects of the field during culture, the temperature of each exposed well was monitored by thermometric probes. The temperature was maintained at $37 \pm 0.1^\circ\text{C}$ throughout the experiments.

Preparation and characterization of RGD–AuNPs. The RGD peptide (NH₂-CYGRGDS-NH₂) was synthesized by a general 9-fluorenylmethoxycarbonyl (Fmoc)-based solid-phase peptide-synthesis strategy. The rink amide AM resin was swelled in DMF for 30 min before use. Fmoc-protected amino acids were activated with HBTU/diisopropylethylamine (HBTU, N,N,N',N'-tetramethyl-O-(1H-benzotriazol-1-yl)uronium hexafluorophosphate) and the coupling reaction was carried out for 1 h. The Fmoc group was removed by treating with 20% (v/v) piperidine/DMF three times after each coupling reaction. The completed peptide was cleaved from the resin by using a mixture of trifluoroacetic acid, ethanethiol, H₂O and triisopropylsilane in the volume ratio of 90/5/2.5/2.5 for 3 h. The peptide was precipitated in cold diethyl ether and purified using preparative HPLC to yield the desired material. The purified peptide was confirmed to be the desired product by liquid chromatography (LC)/MS (expected mass = 755.3 Da; observed mass = 754.3 Da (Supplementary Fig. 1c)). AuNPs of 20 nm were prepared as previously reported³⁴. These were treated sequentially with aqueous mPEG₃₅₀-SH solution (10 mM) and then aqueous RGD peptide solution (10 mM). The RGD–AuNPs were characterized by UV–vis spectroscopy and an absorbance maximum at 535 nm was obtained. DLS measurements indicated a particle size of 35.6 ± 8.8 nm at 25°C , and the surface charge was 16.2 ± 5.2 mV. Each measurement was performed at least three times. The modified AuNPs (28 µg ml⁻¹ RGD–AuNPs in deionized (DI) water) were applied to a gelatine-coated coverglass (2 h in 0.2 wt% gelatine solution in PBS) for 24 h with gentle stirring, rinsed three times with DI water and then dried at room temperature. Field-emission scanning electron microscopy (FESEM) was used to observe the size and morphology of AuNPs that were treated on the gelatine-coated coverglass. The samples were platinum-coated to avoid charging effects and the images were acquired at voltages that ranged from 5 to 15 kV using the FESEM instrument SIGMA from Carl Zeiss.

Cell culture. Mouse TTFs were isolated by removing the mouse tails of eight-week adult mice (ICR mice, Pitx3-eGFP KI) according to standard procedures¹². Human control cells (GM23967, male, healthy control) were purchased from the Coriell Cell Repository. The cell lines were authenticated by short tandem repeat (STR) analysis serviced by Kogenebiotech and were also tested negative for mycoplasma using the MycoSensor PCR Assay Kit (Agilent) every 3 months. The cells were passaged once prior to being pooled and frozen for further use. After thawing, fibroblasts were cultured on 10 cm plates until confluent, and trypsinized for subculture. The medium was replaced every 2 d. To apply the electromagnetized AuNP system, mouse fibroblasts were subcultured on 1.2 cm diameter glass plates coated with gelatine plus AuNPs. Human peripheral blood mononuclear cells (hPBMCs, female, 19 years old, healthy control) derived from human peripheral blood were purchased from Komabiotech (PBM001233). Human PBMCs were plated on Matrigel-coated AuNP coverslips in a PBMC medium, which consisted of DMEM (Invitrogen) that contained 20% fetal bovine serum (FBS, Hyclone), interleukin 6 (ThermoFisher Scientific), interleukin 7 (ThermoFisher Scientific) and penicillin/streptomycin (Invitrogen). After plating for 1 d, the blood cells were transduced with lentivirus that encoded FUW-ASCL1, FUW-PITX3, FUW-NURR1 and FUW-LMX1A and were cultured with PBMC media. After transduction for 3 d, the cells were transferred to N3 medium.

Virus generation. The lentiviral vectors that contained the mouse complimentary DNAs (cDNAs) for FUW-Ascl1, FUW-Pitx3, FUW-Nurr1 and FUW-Lmx1a have been described previously¹². The tracing construct AAV vector for phSyn-FLEX-EGFP-WPRE (Addgene plasmid ID 51504) was purchased from Addgene and the

lentiviral vector for GFAP promoter-Cre was subcloned from Addgene (plasmid ID 40591). The lentivirus generation procedure was performed according to the standard procedures. The cells were co-transfected with the lentivirus constructs psPAX2, pMD2.G and FUW-Ascl1, FUW-Pitx3, FUW-Nurr1, FUW-Lmx1a and GFAP promoter-Cre using calcium phosphate co-precipitation. For the AAV virus generation, we used an AAV helper free system (Agilent Technology). AAV-293 cells were cultured in high-glucose DMEM that contained 10% FBS and 1% penicillin/streptomycin. The cells were co-transfected with the AAV virus construct, pAAV-RC, pHelper and phSyn-FLEX-EGFP-WPRE vectors using the manufacturer's protocol.

Transfection procedure and the plasmid constructs. The expression constructs that contained the mouse cDNAs for Ascl1 (CAG-Ascl1), Pitx3 (CAG-Pitx3), Nurr1 (CAG-Pitx3) and Lmx1a (CAG-Lmx1a) were subcloned from each FUW-TetO vector described previously¹². For the transfection of these factors, the fibroblasts were seeded 24 h before transduction at a density of 75~80%. Three consecutive transfections were performed over a period of 36 h using the FuGENE HD Transfection Reagent (Promega). The constructs were co-transfected with a monolayer of fibroblasts in a six-well culture dish, using 5:2 or 6:2 ratios of FuGENE HD Transfection Reagent to DNA, respectively, and the cells were incubated for 12 h according to the manufacturer's protocol. The culture medium was changed 12 h after the previous transfection.

Cell viability. The cell viability test was performed the standard procedure of a 3-(4,5-dimethylthiazol-2-yl)-2,5-diphenyl tetrasodium bromide (Sigma-Aldrich) assay. Cell viability in the untreated control group was set to 100% for all comparisons.

qRT-PCR. qRT-PCR was carried out as per the standard protocols.

Fluorescence-activated cell sorting (FACS) analysis. To assess the cellular expression of Pitx3-eGFP, we conducted a FACS analysis, performed according to the standard protocols.

Western blot analysis. Western blot analysis was carried out using standard protocols. Antibodies specific to H4K12ac (1:1000, 07-595, Millipore), Brd2 (1:1000, C15310094, Diagenode), H3K27ac (1:1000, 07-360, Millipore), H3K27me3 (1:1000, 07-449, Millipore), H3K4me3 (1:1000, 07-473, Millipore) and β-actin (1:2000, EP1123Y, Millipore) were used.

Immunocytochemistry. Immunocytochemistry analysis was carried out using standard protocols. Antibodies specific to TuJ1 (1:500, AB15708B, Millipore), H4K12ac (1:1000, 07-595, Millipore), MAP2 (1:500, AB5622, Millipore), TH (1:500, P40101-150, Pal-Freez, Rogers), DAT (1:500, MAB369, Millipore), H3K27ac (1:1000, 07-360, Millipore), H3K4me3 (1:1000, 07-473, Millipore) and the appropriate fluorescent secondary antibodies (Invitrogen) were used.

In vivo direct lineage reprogramming in a PD model. All the animal procedures were performed according to institutional ethical guidelines and were approved by the Committee on Animal Welfare of Dongguk University. The procedures employed were carried out following the recommendations from Association for Assessment and Accreditation of Laboratory Animal Care. For all the mouse studies, 12-week-old male C57Bl/6 mice were randomly assigned to receive injections of 6-OHDA/MPTP or saline. For the 6-OHDA PD model, mice were anaesthetized with avertin, placed in a stereotaxic frame and 6-OHDA (10 µg µl⁻¹, dissolved in 0.02% ascorbate/saline) injected into the substantia nigra at coordinates anteroposterior (AP) -3.1 mm, mediolateral (ML) ±1.1 mm and dorsoventral (DV) -4.4 mm for 4 min at a rate of 0.5 µl min⁻¹ using a 26-gauge 10 µl Hamilton syringe. Three weeks after the 6-OHDA injection, the mice were injected intraperitoneally (i.p.) with apomorphine (4 mg kg⁻¹, Sigma) and the rotational behaviour was assessed. Mice that exhibited net anticlockwise turns were lesioned in the left striatum, whereas mice that exhibited net clockwise turns were lesioned in the right (ipsilateral) striatum. Lentivirus that encoded APLN and the AuNPs were injected into the striatum (AP +0.4 mm, ML ±1.5 mm and DV -2.8 mm) and mice were exposed to the EMF conditions for 3 h per day over 4 weeks. Apomorphine-induced rotational behaviour was measured again at 4 and 8 weeks after grafting. The number of clockwise and anticlockwise turns was counted and expressed as the number of net rotations towards the lesioned hemisphere per 60 min. For the MPTP model, mice were injected i.p. with 30 mg kg⁻¹ d⁻¹ MPTP for 8 d or saline once daily for 8 d (i.p., Tokyo Chemical). After the final MPTP injection (8 d), the APLN lentivirus and AuNPs were injected into mouse striatum (AP +0.4 mm, ML ±1.5 mm and DV -2.8 mm), and these mice were exposed to the EMF conditions for 3 h per day over 4 weeks. Mouse behaviours were assessed by ambulation and rearing in the open field. The open-field test is commonly used to investigate anxiety-like behaviours in rodents. Mice were acclimatized for 5 min to an open-field chamber (60 × 60 × 40 cm³) with a defined 20 × 20 cm² central area. At 24 h after habituation, all the mice were placed in one corner of the chamber and allowed to explore the environment for 10 min. The time spent in the centre area and number of line crossings between the square area was hand scored by the experimenter for all mice. The floor surface of the chamber was thoroughly cleaned with 70% alcohol between trials. For rearing

frequency, we observed a rearing rate for 2 min in each mouse. For the genetic tracing experiment, the GFAP-cre mice (The Jackson Laboratory, 024098-B6.Cg-Tg (GFAP-cre)77.6Mvs/2J) were anaesthetized with avertin, placed in a stereotaxic frame and 3.5 µl of lentivirus were co-injected into the striatum region at coordinates AP +0.4 mm, ML ±1.6 mm and DV -2.8 mm for 14 min at a flow rate of 0.25 µl min⁻¹ and a diffusion time of 5 min using a 26-gauge 10 µl Hamilton syringe. The tracing virus phSyn-FLEX-EGFP-WPRE (Addgene plasmid ID 51504) AAV virus (0.7 µl) and reprogramming factors FUW-Ascl1, FUW-Pitx3, FUW-Lmx1A and FUW-Nurr1 lentivirus (0.7 µl each) were injected at the same dilutions and volume and the tracing virus without reprogramming factors was injected in the contralateral side. The titre of viral particles was approximately 10⁸ viral particles per microlitre, which was determined by the transduction of HEK 293 cells. Animals were kept for 8 weeks for the tracing analysis. A 6-OHDA-treated wild-type mouse with reprogramming factors was used for the behaviour rescue experiment (Supplementary Fig. 12e), whereas a GFAP-cre mouse infected with the FLEX-synapsin:GFP virus was used for the genetic tracer experiment (Fig. 6g). We found reduced numbers of GFP/TH double-positive cells in these GFAP-cre mice because the double-positive cells appeared only in the astrocytes, which were infected with both FLEX-GFP and reprogramming factors.

Microarray and ChIP-seq analysis. The microarray analysis was conducted using an Illumina MouseRef-8 v2 Expression BeadChip following the manufacturer's instructions. The quantile normalization method was used and probes differentially expressed in at least 50% of the arrays were kept according to a detection *P* value less than 0.05. Functional-enrichment analysis was performed using a GOSTate (Falcon and Gentleman) *R* package. For ChIP sequencing, DNA libraries were constructed using the KAPA library preparation kit (Illumina) according to the manufacturer's instructions. Sequencing was implemented on Illumina HiSeq2000. Trimmomatic v 0.33 (ref. 35) was applied to remove the Illumina adapter as well as to trim and crop the sequencing data. The reads were aligned to the mouse genome (mm10) using Bowtie v 1.1.2 (ref. 36), and only uniquely mapped reads in the genome were used for downstream applications. Heat maps and plots of average enrichments for the ChIP-seq data were generated by DeepTools v. 1.5 (ref. 37) applying *k*-means clustering (*k* = 3). Bigwig files were also created by DeepTools and visualized by the UCSC genome browser. ChIP-seq peaks were identified by MACS v 1.4.2 (ref. 38) using broad-peak calling analysis (shift size 73) and the annotations of the called peaks were determined using the ChIPseeker³⁹ *R* package. For the CellNet-based GSEA, we downloaded the database of GRNs for neurons, fibroblasts and ES cells from CellNet and gene-enrichment patterns were generated by the GSEA^{40,41} pre-ranked mode using a ranked log2-fold change and GRNs in CellNet⁴². The normalized enrichment score (NES), nominal *P* value and false discovery rate (FDR) are indicated in each enrichment plot.

In vitro electrophysiology. For electrophysiological analysis, patch pipettes were filled with (in mM) 110 potassium gluconate, 20 KCl, 2 Mg-ATP, 10 sodium phosphocreatine, 1.0 EGTA, 0.3 GTP-Tris and 20 HEPES (pH 7.25, 320 mOsm). Electrodes were fabricated from borosilicate capillary glass tubing (Warner Instruments) by a capillary glass puller (Sutter Instruments) and polished on a microforge (Narishige) to a resistance of 2~4 MΩ. After establishing the whole-cell mode, the cell-membrane capacitance and series resistance were compensated to 75% electronically using a patch-clamp amplifier (Axopatch 200B, Molecular Devices). Data acquisition was performed using pClamp10 software on an IBM computer equipped with an ADC (Digidata 1440A, Axon Instruments). Action potentials were elicited from iDA neurons 15 d after transfection/transduction with APLN. Recordings were started on day 14 based on the neuron-like morphology, including rounded cell bodies and the presence of branched and extended neurites. Fast inward sodium currents and outward potassium currents were measured in voltage-clamp mode with voltage-step protocols that ranged from -55 to +55 mV. To confirm the recorded cells, biocytin (0.2%) was added to the intracellular medium and the neuronal identity of the analysed cells was confirmed by double immunostaining of TH and biocytin.

Electrophysiological activities of *in vivo* converted neurons. To evaluate the electrophysiological activities of *in vivo* converted neurons, patch-clamp recordings were performed on brain slices. To identify *in vivo* converted neurons on the brain slice, AuNPs in solution along with lentiviral APLN factors, GFAP-Cre (Cre expression under the control of the GFAP promoter) and AAV virus for Flex-synapsin:GFP (GFP expression under the synapsin promoter in Cre-positive cells) were transplanted into the MPTP or the 6-OHDA-treated striatum, and the mice were then exposed to EMF. After 8 weeks of conversion, the brain was quickly removed and transferred into cold artificial cerebrospinal fluid (ACSF) ((in mM) 117 NaCl, 3.6 KCl, 2.5 CaCl₂, 1.2 MgCl₂, 1.2 NaH₂PO₄, 25 NaHCO₃ and 11 glucose) aerated with 95% O₂-5% CO₂ under isoflurane anaesthesia. The brain was then sliced coronally at 300 µm thickness through the striatum using a Vibratome (Leica, VT1200S). The slices were kept for 1 h in ACSF at 34 °C, transferred to the recording chamber on the stage of a BX51W1 microscope and perfused with ACSF (2 ml min⁻¹) at room temperature. GFP-labelled converted cells were identified under a fluorescence microscope and then visualized by using infrared differential

interference contrast optics at ×40 magnification for whole-cell configurations. Recordings were performed in a voltage-clamp mode using a Multiclamp 700B amplifier (Axon Instruments) and pCLAMP 10 data-acquisition software (Molecular Devices). The patch-pipettes (5–6 MΩ) were backfilled with internal solution that contained the following (in mM): 120 K-gluconate, 10 KCl, 2 Mg-ATP, 0.5 Na-GTP, 0.5 EGTA, 20 HEPES, 10 phosphocreatine. Spontaneous EPSCs were recorded at a holding potential of -70 mV. In every voltage clamp recording, an equilibration period of 5–10 min was allowed after whole-cell access was established, and the recording reached a steady state. After 5 min of baseline recording, 20 µM CNQX and 50 µM D-AP5 (Sigma) in ACSF were perfused for 10 min.

DA measurement. DA was determined by an API 3200 triple quadrupole mass spectrometer system (Applied Biosystems) and carried out as in the standard protocol.

Vibrating sample magnetometer (VSM) measurement. Using a non-magnetic Quartz rod, AuNP samples were measured by the VSM option of the Physical Properties Measurement System (PPMS-Dynacool 14 T magnet, Quantum Design). The experimental conditions were 300 K with the hysteresis curve about -0.5 to 0.5 T.

Statistical analysis. All the data are presented as the mean ± s.d. of three independent experiments. *n* values indicate the number of independent experiments performed or the number of individual experiments or mice. For each independent *in vitro* experiment, at least three technical replicates were used and a minimum number of three independent experiments were performed to ensure an adequate statistical power. Group differences were considered statistically significant at *P* < 0.05 (**P* < 0.05, ***P* < 0.01). An analysis of variance (ANOVA) test was used for multicomponent comparisons and a Student's *t*-test for two-component comparisons after the normal distribution was confirmed. For the animal studies, no or weak (<80%) behaviour phenotypes of mice 4 weeks after the drug (MPTP or 6-OHDA) treatment were deemed as technical failures and were excluded from further analysis. This occurred in ~5% of cases. After 6-OHDA/MPTP treatment, two groups of either sham-operated or lesioned-only mice were matched and served as controls. All the MPTP- and 6-OHDA-treated mice were randomly selected for the experimental groups further treated under the electromagnetized conditions. EMF-treated mice were monitored daily, and animals with poor post-surgical recovery or signs such as dyspnoea and inactivity were also excluded. This occurred in ~5% of cases. Behaviour and image analyses were blinded and performed by independent investigators. Histological analyses were blinded and performed by an independent investigator.

Data availability. The data that support the plots within this paper and other findings of this study are available from the corresponding author on reasonable request. The microarray data cited in Fig. 3 have been deposited in the NCBI GEO database under the accession code GSE86052.

References

32. Hei, W. H. *et al.* Schwann-like cells differentiated from human dental pulp stem cells combined with a pulsed electromagnetic field can improve peripheral nerve regeneration. *Bioelectromagnetics* **37**, 163–174 (2016).
33. Loginov, V. Accumulation of calcium ions in myocardial sarcoplasmic reticulum of restrained rats exposed to the pulsed electromagnetic field. *Aviakosm. Ekolog. Med.* **26**, 49–51 (1991).
34. Bastus, N. G., Comenge, J. & Puntes, V. Kinetically controlled seeded growth synthesis of citrate-stabilized gold nanoparticles of up to 200 nm: size focusing versus Ostwald ripening. *Langmuir* **27**, 11098–11105 (2011).
35. Bolger, A. M., Lohse, M. & Usadel, B. Trimmomatic: a flexible trimmer for Illumina sequence data. *Bioinformatics* **30**, 2114–2120 (2014).
36. Langmead, B., Trapnell, C., Pop, M. & Salzberg, S. L. Ultrafast and memory-efficient alignment of short DNA sequences to the human genome. *Genome Biol.* **10**, R25 (2009).
37. Ramírez, F., Dündar, F., Diehl, S., Grüning, B. A. & Manke, T. deepTools: a flexible platform for exploring deep-sequencing data. *Nucleic Acids Res.* **42**, W187–W191 (2014).
38. Zhang, Y. *et al.* Model-based analysis of ChIP-seq (MACS). *Genome Biol.* **9**, 1 (2008).
39. Yu, G., Wang, L.-G. & HeQ.-Y. ChIPseeker: an R/Bioconductor package for ChIP peak annotation, comparison and visualization. *Bioinformatics* **31**, 2382–2383 (2015).
40. Mootha, V. K. *et al.* PGC-1α-responsive genes involved in oxidative phosphorylation are coordinately downregulated in human diabetes. *Nat. Genet.* **34**, 267–273 (2003).
41. Subramanian, A. *et al.* Gene set enrichment analysis: a knowledge-based approach for interpreting genome-wide expression profiles. *Proc. Natl Acad. Sci. USA* **102**, 15545–15550 (2005).
42. Cahan, P. *et al.* CellNet: network biology applied to stem cell engineering. *Cell* **158**, 903–915 (2014).